

Highly Efficient and Selective Hydrodeoxygenation of Guaiacol Using Ni-Supported Honeycomb-Structured Biochar and Phosphomolybdic Acid

Tao Yin,^[a] Yang Luo,^[a] Ripsa Rani Nayak,^[b] Riyang Shu,^{*[a]} Zhipeng Tian,^[a] Chao Wang,^[a] Ying Chen,^[a] and Navneet Kumar Gupta^{*[b]}

The sustainable development of energy has always been a concern. Upgrading biomass catalysis into hydrocarbon liquid fuels is one of the effective methods. In order to upgrade biomass derivative guaiacol by Hydrodeoxygenation (HDO) catalysis, this article reports a three-dimensional honeycomb structure biochar loaded with Ni nanoparticles and phosphomolybdic acid demonstrating excellent catalytic performance in a short period of time. This is due to the porous structure of biochar, which allows Ni metal nanoparticles to be highly uniformly dispersed on the support, which enhances the catalytic hydrogenation of guaiacol in terms of both rate and efficiency. Furthermore, it was observed that the added phosphomolybdic acid dissolved within the temperature range

of 78–90 °C, functioning as a homogeneous catalyst in the process. This proves advantageous, as the phosphomolybdic acid becomes accessible at any location within the porous Ni/C catalyst. The detailed characterization data revealed that the carbon support prepared in this study has a high specific surface area of up to 1375.61 m²/g. Additionally, the phosphomolybdic acid exhibited rich acidity, with Brønsted and Lewis acid contents of 2.55 μmol/g and 21.45 μmol/g, respectively. Reaction data demonstrated that at 240 °C for 180 min, 100% conversion and 97.9% cyclohexane selectivity were achieved. This study introduces a bifunctional catalyst with a unique catalyst's structure, facilitating a heterogeneous-homogeneous catalytic reaction and delivering an efficient catalytic effect.

1. Introduction

As the world continues to develop rapidly, challenges related to energy and the environment are becoming increasingly urgent. This has heightened the need for green, high-value renewable energy sources.^[1] Lignin is the largest renewable source of aromatic hydrocarbons in nature, and due to its rich aromatic hydrocarbon structure, it is often used in various catalysis applications. The unique cyclic conjugated structure of aromatic compounds gives them high stability and the ability to withstand certain reaction conditions without easily decomposing. Secondly, due to the structural characteristics of aromatic compounds, they often have high reaction selectivity in catalytic reactions. Directional conversion of the target product can be achieved through appropriate catalysts and reaction conditions. Aromatic compounds have great potential as raw materials for producing high value-added products and liquid fuels.^[2–4] Lignin, when pyrolyzed, produces bio-oil rich in benzene ring structural units – an eco-friendly and cost-

effective resource. Hydrodeoxygenation (HDO) can enhance the carbon-to-hydrogen ratio in these benzene rings while reducing their oxygen content, enabling their conversion into high-energy aromatic and cycloalkane liquid fuels.^[5–8] Model compounds commonly found in bio-oil, such as guaiacol, phenol, and vanillin, are often used in HDO experiments to explore their potential for further upgrading.^[9–11]

In HDO catalytic studies, catalyst supports are typically categorized into carbon, metal oxides, silica, etc.^[12] Carbon supports are favored for their green credentials, abundant precursor resources, developed pore structures, strong adsorption properties, good thermal stability, and minimal environmental impact.^[13–15] Metal supports offer benefits like excellent thermal stability and easy recycling but often require high reaction temperatures for the reaction.^[16,17] Silicon oxide supports are known for their high porosity, multiple surface-active centers, and acid resistance, though they suffer from low mechanical strength and susceptibility to sintering.^[18] Therefore, selecting the appropriate support involves carefully balancing these advantages and disadvantages.

The hydrogenation reaction during the hydrodeoxygenation process is closely linked to the type of metal loaded onto the support. Previous studies have shown that precious metals exhibit exceptionally high catalytic activity. Typically, precious metals such as Pt, Ag, Pd, and Ru are employed in research. For example, Li et al. achieved effective catalytic results for phenol HDO using Pt-supported TiO₂ nanosheets at 50 °C and atmospheric H₂ pressure.^[19] Similarly, Lup et al. demonstrated good benzene selectivity with Ag/TiO₂ catalysts for phenol HDO.^[20] Teles et al. investigated the impact of different supports on the

[a] T. Yin, Y. Luo, R. Shu, Z. Tian, C. Wang, Y. Chen
 Guangdong Provincial Key Laboratory of Functional Soft Condensed Matter,
 School of Materials and Energy, Guangdong University of Technology,
 Guangzhou 510006, PR China
 E-mail: shuriyang@gdut.edu.cn

[b] R. R. Nayak, N. K. Gupta
 Centre for Sustainable Technologies, Indian Institute of Science, Gulmohar
 Marg, Mathikere, Bengaluru 560012, India
 E-mail: nkgupta@iisc.ac.in

Supporting information for this article is available on the WWW under
<https://doi.org/10.1002/asia.202400999>

HDO performance of Pd-based catalysts with various model molecules (phenol, m-cresol, benzyl ether, guaiacol) at 300 °C, finding that Pd/NbO and Pd/NbOPO catalysts exhibited excellent HDO activities.^[21] Shu et al. prepared Ru/TiO₂-CeO₂ using a photochemical reduction method and achieved 100% selectivity for cyclohexane in the HDO of lignin phenolic compounds at 230 °C and 1 MPa H₂ for 4 h.^[22] While precious metals have demonstrated outstanding catalytic performance, their scarcity and high cost are significant drawbacks. As a result, research has shifted towards transition metals, which are more abundant and cost-effective. Ni, in particular, has emerged as a promising alternative due to its favorable price and catalytic activity comparable to that of precious metals. For instance, Novodárszki et al. reported a cyclohexane yield of about 90% using Ni metal loaded on Al₂O₃ at 250 °C and 0.1 MPa H₂.^[23] Zhang prepared a flower-shaped radial channels Ni₂P@C/FLRC-TiO₂-1 catalyst, which achieved 100% conversion of cresol and 93.7% selectivity for methylcyclohexane (MCH) within 1.5 h at 275 °C and 2 MPa H₂.^[24]

The effectiveness of the deoxygenation process in HDO catalytic reactions is significantly influenced by the acidic sites of the catalyst.^[25] The type and quantity of these acidic sites play a crucial role in determining the efficiency of HDO. Typically, acidic sites can be introduced by adding acidic compounds or Al₂O₃ material. For instance, Chen et al., utilized a dual-functional catalyst combining phosphotungstic acid with Pd/SiO₂ to efficiently hydrogenate and deoxygenate biomass-derived furanics. The inclusion of phosphotungstic acid introduced abundant Brønsted and Lewis acidic sites, which synergistically enhanced the reaction for HDO over Pd metal sites.^[26] Dutta et al. explored the interaction between Ni and Al₂O₃ supports, revealing that benzyl ether interacts with the acidic sites of Al₂O₃. The study found that hydrogenation of aromatic rings was primarily controlled by Ni sites in the presence of H₂, while demethylation occurred during adsorption on Al₂O₃.^[27]

Therefore, in this study, we propose that Ni/C can effectively facilitate the HDO reaction when combined with heteropolyacid. The porous structure of the biomass-derived carbon support not only ensures high dispersion of Ni metal but also enhances the adsorption of reaction substrates, enabling the reaction to proceed rapidly. Phosphomolybdic acid, being a homogenous liquid during the reaction, can easily interact with any part of the carbon support to create acidic sites, thereby promoting the completion of the HDO process. Additionally, HDO performance tests conducted with various model compounds from lignin derivatives and bio-oils using this catalyst demonstrated excellent catalytic activity.

Experimental

Materials

The chemicals used in this experiment include n-octane (> 99%), guaiacol (> 99%), potassium carbonate (99%, K₂CO₃), phosphomolybdic acid (99%, H₃PMo₁₂O₄₀·13H₂O), molybdic acid (99%, H₂MoO₄), phosphoric acid (> 85%, H₃PO₄), tungstic acid (99%,

H₂WO₄), silicotungstic acid (99%, H₄[Si(W₃O₁₀)₄]), and other model compounds, all of which are AR grade and were purchased from Camaro. The peanut shell precursor was sourced from Lianyungang, Jiangsu. Lignin bio-oil was obtained by pyrolyzing rice husks in a laboratory tube furnace to produce primary bio-oil, which was then separated into the required phenolic compounds through fractional distillation and condensation.

Methods

Catalyst Preparation

Peanut shells, K₂CO₃, and water are mixed in a mass ratio of 1 : 1.5 : 4 to form a slurry, which is then stirred and dried in an oven at 80 °C. After drying, the mixture is ground into a uniform powder and subjected to pyrolysis in a tube furnace. The pyrolysis is conducted under a N₂ atmosphere (80 ml/min) with a heating rate of 5 °C/min, reaching a target temperature of 800 °C, and maintained for 90 min. The resulting preliminary biochar is then ground into a fine powder, boiled in DI water at 100 °C for 2 h, and subsequently filtered. After cooling to room temperature, the biochar is dried and ground again to yield a biochar support with a high specific surface area and well-developed pore structure. Biochar is referred to as C for simplicity.

The Ni-based biochar carrier is prepared by stirring 1 g of the dried biochar, 1 g of nickel nitrate hexahydrate, and 30 g of deionized water at room temperature in a beaker for 12 h at 300 rpm. The mixture is then dried, ground, and subjected to heating and reduction in a H₂ atmosphere at 600 °C for 70 min to obtain Ni/C.

HDO of Lignin-Derived Phenolic Compounds: Experimental Setup and Catalytic Performance

The HDO reaction was conducted in a 35 mL 316 L stainless steel four-station reaction vessel from Guizhou Shanli Experimental Instrument Company. Typically, 50 mg of phenolic model compound, 42 mg of Ni/C catalyst, and 20 mg of H₃[P(Mo₃O₁₀)₄]⁻¹³H₂O were used. The model compound and catalyst were added to the reaction vessel, followed by 10 mL of octane solvent. The vessel was purged with 1 MPa H₂ for 10 s to remove impurities and ensure a purified reaction atmosphere. The mixture was then heated to a specified temperature (230–250 °C) with stirring at 400 rpm.

Gas chromatography (GC-2014 C AT, Shimadzu, Japan) with a thermal conductivity detector (TCD) was used to analyze the gas-phase products using N₂ as the carrier gas. The liquid-phase products were analyzed using gas chromatography-mass spectrometry (GC-MS) on a Thermo Fisher Science Trace1300, with a TG-5Sil chromatographic column. The oven temperature was programmed to start at 60 °C for 2 min, then increased to 260 °C at a rate of 10 °C/min and held for an additional 10 min. The syringe was maintained in split mode at 280 °C (5 : 1) with He as the carrier gas. Quantitative determination was performed using a reconstructed flame ionization detector (FID) on the same instrument. Internal standards for typical phenolic compounds such as guaiacol, cyclohexane, cyclohexanol, and 2-methoxycyclohexanol were prepared for the GC calibration. The conversion rate and product selectivity of phenolic compounds were calculated using the formulas provided in Equations (1 and 2), and similar calculations were applied to bio-oil and other model compounds.

$$\text{Conversion (\%)} = (\text{moles}_{\text{in}} - \text{moles}_{\text{out}}) / \text{moles}_{\text{in}} \times 100\% \quad (1)$$

$$\text{Selectivity (\%)} = \text{moles}_{(\text{product})i} / \sum \text{moles}_{(\text{product})} \times 100\% \quad (2)$$

Catalyst Characteristics

X-ray diffraction (XRD) was used to determine and analyze the phase stability of C, Ni/C, and $\text{H}_3\text{PMo}_{12}\text{O}_{40}\cdot 13\text{H}_2\text{O}$ catalysts within the diffraction angle range of 2θ from 8° – 85° . Scanning electron microscope (SEM) and Energy dispersive spectroscopy (EDS) were used to analyze the morphology, Ni distribution, and elemental composition of biochar, Ni supported biochar, and phosphomolybdic acid. Brunauer-Emmett-Teller (BET) was used to measure the N_2 adsorption-desorption data to analyze the specific surface area and pore size data. Transmission electron microscopy (TEM) was used to observe Ni on Ni supported biochar to determine particle size. The H_2 adsorption and desorption behavior of Ni/C was tested using H_2 -TPD programmed heating to understand the activity of the catalyst and the dispersion of Ni metal on the catalyst surface. For the detection of acidic sites in bifunctional catalysts, infrared pyridine was used to measure the acidity type.

2. Results and Discussions

2.1. Physicochemical Characterization of Catalysts

XRD analysis was conducted to characterize C, Ni/C, and $\text{H}_3\text{PMo}_{12}\text{O}_{40}\cdot 13\text{H}_2\text{O}$. As depicted in Figure S1, the carbon carrier shows a slightly prominent peak around 23° , characteristic of amorphous carbon.^[28] The Ni/C catalyst displays distinct Ni peaks at (111), (200), and (220), with no impurity peaks, indicating high purity and single-phase nickel nanoparticles.^[29] Analysis of the phosphomolybdic acid using Jade software reveals clear characteristic peaks corresponding to $\text{H}_3\text{PMo}_{12}\text{O}_{40}\cdot 13\text{H}_2\text{O}$, with some impurity peaks observed beyond 45° .

C, Ni/C, and $\text{H}_3\text{PMo}_{12}\text{O}_{40}\cdot 13\text{H}_2\text{O}$ were characterized using SEM and EDS. As shown in Figure S2 (a), biochar (C) exhibits a three-dimensional honeycomb structure, highlighting its excellent pore architecture. This structure is consistent with the BET test data discussed later, which confirms that the porous nature of C facilitates effective loading of Ni metal onto the carbon support. Figures S2 (b–d), reveal numerous small spherical particles uniformly distributed on the large pore walls of the carbon support, identified by EDS as Ni metal. Figures S2(e–i)

illustrate the morphology and elemental composition of $\text{H}_3\text{PMo}_{12}\text{O}_{40}\cdot 13\text{H}_2\text{O}$.

Table S1 shows the BET data for C and Ni/C. The results indicate that C has a high specific surface area of $1375.61\text{ m}^2/\text{g}$, a total pore volume of $1.089\text{ cm}^3/\text{g}$, and a mesoporous pore volume of $0.4187\text{ cm}^3/\text{g}$. In contrast, the Ni/C sample shows reduced values compared to C, attributed to the occupation of mesopores and micropores by Ni metal.^[30] The isothermal adsorption-desorption curve shown in Figure S3 is of type-IV, exhibiting a hysteresis loop that confirms the presence of mesopores.

Figure 1 shows the TEM characterization of Ni/C, revealing that Ni metal exhibits uniform particle size and good dispersion, with particles primarily around 8.16 nm. This uniform dispersion of Ni metal enhances the hydrogenolysis and hydrogenation reactions during the HDO process, thereby improving reaction efficiency. Additionally, the small size of Ni particles positively impacts the HDO process, further contributing to enhanced reaction performance.^[31]

Additionally, H_2 -TPD characterization was employed to analyze Ni/C, with the hydrogen desorption curve fitted based on the experimental data shown in Figure S4. A distinct hydrogen desorption peak is observed at a lower temperature of 119.1°C , which corresponds to hydrogen adsorbed on the surface of Ni species. This low-temperature peak indicates that hydrogen species adsorbed on the exposed Ni surface can desorb at relatively low temperatures. The uniform distribution of Ni metal on the C support facilitates faster hydrogen adsorption. The adsorption equilibrium is reached when the peak starts to decline after 391.4°C .^[32,33]

In the HDO process, acidic sites are crucial for removing oxygen-containing groups from the carbon ring. Pyridine infrared (Py-IR) characterization was used to quantify the acidity and type of the Ni/C– $\text{H}_3[\text{P}(\text{Mo}_3\text{O}_{10})_4]\cdot 13\text{H}_2\text{O}$ catalyst, aligning the testing conditions with those used in the HDO reaction. As shown in Table 1, Brønsted acid sites represent 19% of the total acid content, while Lewis acid sites amount to $21.45\text{ }\mu\text{mol}/\text{g}$. Brønsted acids facilitate HDO by weakening C–O bonds through protonation of OH groups, significantly enhancing activity. The presence of abundant Lewis acid sites further supports C=O hydrogenation and C–O cleavage, accelerating the HDO

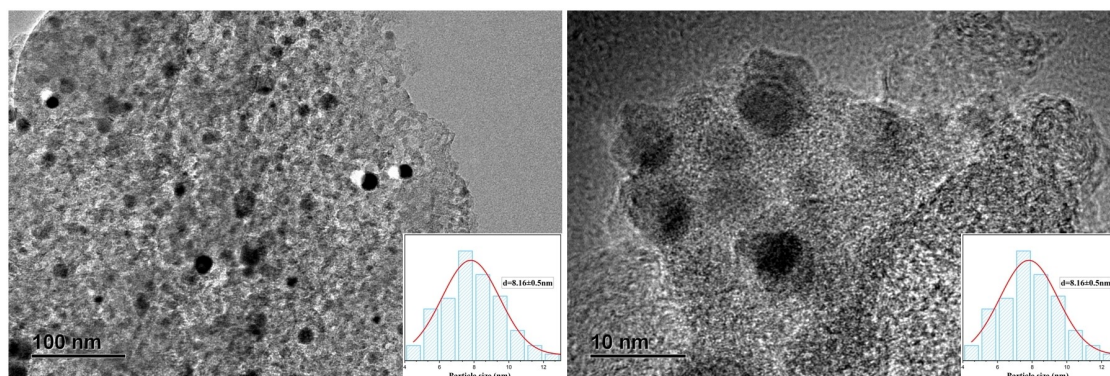


Figure 1. TEM images of the Ni/C. The mean Ni diameter was calculated using $d_{\text{TEM}} = \sum \text{Ni} \cdot d_i^3 / \sum \text{Ni} \cdot d_i^2$, where Ni is the number of metals having diameter d_i ($n > 200$).

Table 1. Distribution of acidic sites in Ni/C–H₃PMo₁₂O₄₀·13H₂O catalyst as determined by Py-IR spectroscopy.

Catalyst	Acidity (μmol/g)		
	Brønsted	Lewis	B/L
Ni/C–H ₃ PMo ₁₂ O ₄₀ ·13H ₂ O	2.55	21.45	0.12

process.^[34,35] The dual presence of these acidic sites in the catalyst markedly improves reaction efficiency.

2.2. Results of Catalytic HDO Experiments

2.2.1. Catalytic HDO of Guaiacol


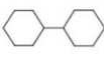
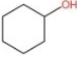
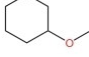
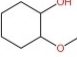
The catalytic HDO performance of various catalysts on guaiacol has been systematically explored. This analysis includes a comparison of the HDO effects of Ni/C in conjunction with different acidic components, such as those found in phosphomolybdic acid and other common heteropolyacids. The experimental results are summarized in Table 2.

The experimental data reveals that the Ni/C–H₃[P(Mo₃O₁₀)₄]-13H₂O catalyst exhibits a superior HDO performance (Table 2, entry 1). The main products of guaiacol HDO include cyclohexane, bicyclic hexane, methoxycyclohexane, cyclohexanol, and methoxycyclohexanol. Variations in product distribution among different catalysts are observed. Specifically, the catalyst used in this study achieves efficient and selective production of cyclohexane when reacting at 240 °C for 180 min. The formation of minor bicyclic hexane is likely due to side reactions such as dehydroxylation, methylation, methoxylation, and condensation during the hydrogenation deoxygenation of guaiacol. In contrast, Ni/C–H₂MoO₄ and Ni/C–H₃PO₄ catalysts performed less effectively (Table 2, entries 2 and 3). This suggests that the molybdic acid and phosphoric acid do not provide effective acidic sites on the support, resulting in suboptimal synergy with the metal sites and a reduced HDO catalytic performance. Heteropolyacid catalysts, such as those used in entries 4 and 5 of Table 2, exhibit stronger acidity and

higher catalytic activity compared to traditional acidic catalysts. This significantly enhances the conversion rate and product selectivity for guaiacol. While entry 5 shows a cyclohexane selectivity of 89.7%, it is still lower than the 97.9% selectivity achieved with Ni/C–H₃[P(Mo₃O₁₀)₄]-13H₂O. In addition, we also studied the catalytic effect of metal sites on acidic sites alone. From entries 6 and 7 in Table 2, we can see that under Ni/C conditions, the products of guaiacol only have 28.7% cyclohexanol and 71.3% methoxycyclohexanol, without good deoxygenation performance. Under the action of H₃[P(Mo₃O₁₀)₄]-13H₂O/C catalyst, guaiacol does not undergo conversion, which may be due to the presence of the C=C double bond, which enhances the C–O bond. When the C=C double bond is opened, the C–O bond weakens, which is beneficial for the deoxygenation process, consistent with the experimental data of time and temperature conditions discussed later. The effective synergy between metal sites, acidic sites, Ni/C, and heteropolyacid in the catalyst substantially improves the HDO catalytic effect.

In parallel with our experimental work, we reviewed recent literature on guaiacol HDO to contextualize our findings. Several studies have explored various catalysts and conditions for this process. For instance, the Mo₂N@NC catalyst, synthesized in situ using a one-step method, demonstrated an impressive guaiacol conversion rate of 99.9% and an aromatic selectivity of 80.2% at 380 °C, 2 MPa H₂, and 0.3 h.^[36] Similarly, Khani et al. utilized Al-MIL-53 MOF impregnated with 3 wt % Ru, achieving 100% guaiacol conversion and a cyclohexane selectivity of 96.2% under conditions of 250 °C, 4 h, and 3 MPa H₂.^[37] Zhang et al. investigated Fe and Ni catalysts, revealing that the Fe₁₀Ni₁/h-BN (10%) catalyst achieved over 98% guaiacol conversion and 98.4% selectivity for cycloalkanes at 300 °C and 3 MPa H₂.^[38] Additionally, Chen et al. explored NiCoAl catalysts with a spinel structure, finding that a calcination temperature of 600 °C was optimal. Under conditions of 250 °C, 1 MPa H₂, and 4 h, this catalyst achieved complete guaiacol conversion with 97.96% selectivity for cyclohexane and 2.04% for cyclohexanol.^[39] Comparing these results with our own, the catalyst developed in this study demonstrates superior perform-

Table 2. Effect of Various Catalysts on Guaiacol HDO.

Entry	Catalysts	Conversion (%)	Product selectivity (%)				
							
1	Ni/C–H ₃ [P(Mo ₃ O ₁₀) ₄]-13H ₂ O	100	97.9	5.2	0	0	0
2	Ni/C–H ₂ MoO ₄	6.8	0	0	49.3	0	50.7
3	Ni/C–H ₃ PO ₄	55	13.1	0	27.6	0	59.3
4	Ni/C–H ₂ WO ₄	100	60.9	0	7.6	3.2	28.3
5	Ni/C–H ₄ [Si(W ₃ O ₁₀) ₄]-xH ₂ O	100	89.7	10.3	0	0	0
6	Ni/C	86.9	0	0	28.7	0	71.3
7	H ₃ [P(Mo ₃ O ₁₀) ₄]-13H ₂ O/C	0	0	0	0	0	0

Reaction conditions: 50 mg guaiacol, 42 mg Ni/C (20 wt% Ni loading), 20 mg acid dosage, 10 mL octane, 240 °C, 1 MPa H₂, 3 h.

ance in terms of product selectivity and efficiency under similar or even milder reaction conditions.

In addition to evaluating catalyst performance, the influence of reaction temperature and time on the HDO of guaiacol using Ni/C-H₃[P(Mo₃O₁₀)₄]*13H₂O was investigated. Both factors significantly affect catalyst efficacy. Each experiment was repeated three times to ensure the accuracy and stability of the experimental data. As depicted in Figure 2, guaiacol achieves 100% conversion across a temperature range of 220–250 °C. Notably, the selectivity for cyclohexane starts at 37.3% at 220 °C but rises sharply to 94.8% at 230 °C. At 240 °C, cyclohexane selectivity reaches 97.9%, and by 250 °C, it attains 100%. This indicates a positive correlation between temperature and cyclohexane selectivity, suggesting that higher temperatures enhance the HDO process. Regarding reaction time, it plays a crucial role in determining the efficiency of guaiacol HDO. By

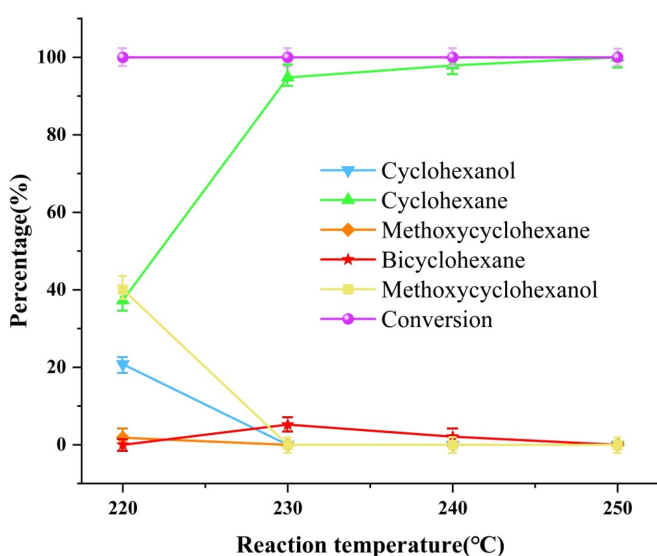


Figure 2. Influence of Reaction Temperature on Guaiacol HDO.

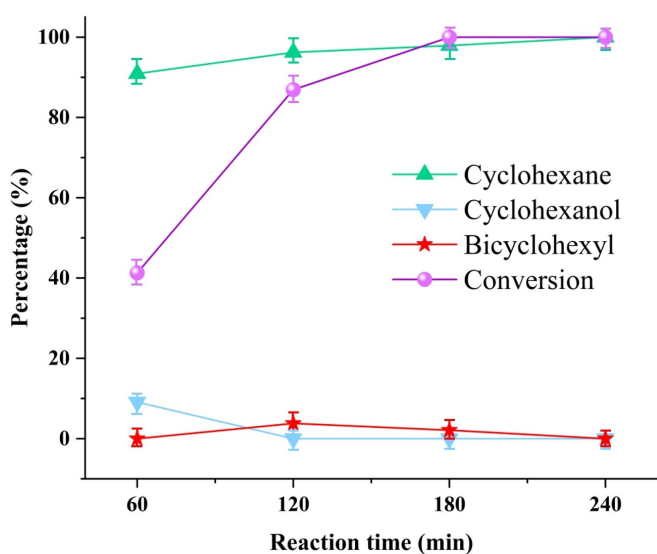


Figure 3. Influence of Reaction Time on Guaiacol HDO.

analyzing the product distribution over various time periods, in conjunction with reaction temperature data, we can infer the reaction mechanism and identify the optimal reaction duration. This comprehensive analysis provides insights into maximizing catalytic performance and achieving the desired product selectivity.

Figure 3 illustrates that the conversion rate initially increases but does not reach 100% within the first 1–2 h of reaction, showing a significant rise from 41.3%–86.9%. The optimal conversion rate and selectivity are achieved after 3 h of reaction time. Thus, the ideal conditions for this experiment are determined to be a reaction temperature of 240 °C and a duration of 3 h.

When analyzing the combined data, it becomes evident that during shorter reaction times at 240 °C, only cyclohexane and cyclohexanol are produced. In contrast, at lower temperatures, the products include cyclohexane, cyclohexanol, methoxycyclohexanol, and a smaller amount of methoxycyclohexane. This observation provides insights into the reaction mechanism, illustrated in Figure 4. Initially, guaiacol adsorbs onto the carrier and undergoes hydrogenation at Ni metal sites, resulting in the formation of methoxycyclohexane. Subsequently, methoxycyclohexanol interacts with the acidic sites near the metal sites, leading to demethoxylation and the production of cyclohexanol, water, and methane. Finally, cyclohexanol is dehydroxylated at the acidic sites to yield the final product, cyclohexane.

In addition, the stability of the catalyst is an important parameter for evaluating its performance, and we conducted five cyclic experiments. From Figure 5, it can be seen that after five experiments, the conversion rate of guaiacol and the selectivity of cyclohexane are still above 80%. It can be seen that the catalyst prepared in this experiment has good stability performance.

2.2.2. HDO Catalysis with Various Model Compounds and Bio-Oil

Based on the experimental data presented, the Ni/C-H₃[P(Mo₃O₁₀)₄]*13H₂O catalyst demonstrates exceptional performance in HDO. Further investigations into the HDO of various model compounds using this catalyst reveal promising results. As depicted in Figure 6, the catalyst achieves a 100% conversion rate for simpler guaiacol derivatives such as cyclohexanol, methoxycyclohexane, and methoxycyclohexanol, along with high selectivity for cyclohexane. Other model compounds including phenol, benzyl ether, propyl guaiacol, and benzofuran also show complete conversion with cycloalkane selectivity. Notably, benzofuran, though complex, exhibits significant cycloalkane selectivity with only 19.4% residual oxygen-containing compounds. Comparative studies further highlight the efficacy of the Ni/C-H₃[P(Mo₃O₁₀)₄]*13H₂O catalyst. Xiang et al. utilized a bifunctional catalyst (0.5Ru₂@5 W₁/ZrO₂) for phenol HDO, achieving 100% cyclohexane selectivity at 250 °C, 2 h, and 3 MPa H₂.^[40] Similarly, Xu et al. employed a Ni–Nb₂O₅ nano catalyst prepared via the sol-gel method for

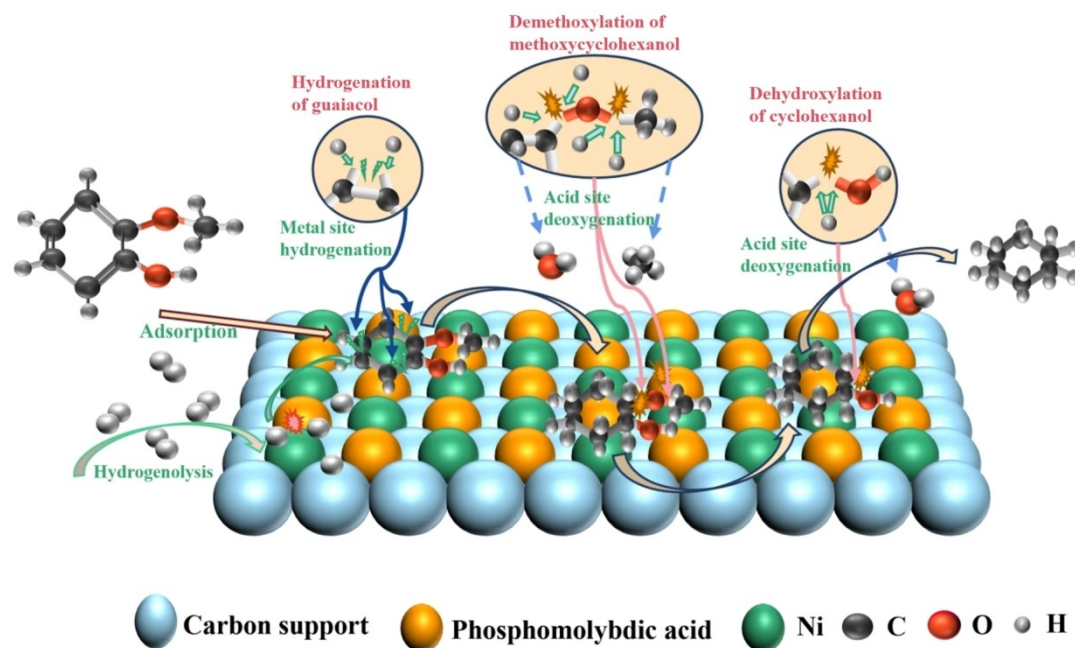


Figure 4. Proposed reaction mechanism of guaiacol HDO.

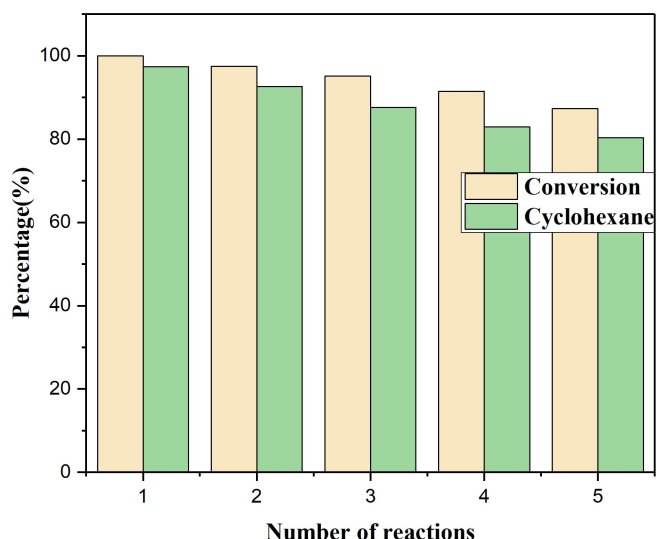


Figure 5. Catalyst stability test

anisole HDO, requiring 240 °C, 3 MPa H₂, and 4 h to fully convert benzyl ether to cyclohexane.^[41] Pérez et.al research on Ni–Mo catalysts loaded into multi-walled carbon nanotubes (CNTs) demonstrated a high deoxygenation yield of 93.8% for benzofuran after 4 h at 320 °C, with a major product yield of 74% ethylcyclohexane (ECH).^[42] In comparison, the reaction conditions used in this study are relatively mild, underscoring the efficiency and effectiveness of the Ni/C- H₃[P(Mo₃O₁₀)₄]-*13H₂O catalyst.

We also examined the HDO performance of lignin bio-oils, which present a more complex composition and greater challenges due to their high content of oxygen-containing and unsaturated groups. These characteristics hinder the conversion

and upgrading of lignin bio-oil into liquid fuel. As depicted in Table S3, the lignin bio-oil used in this study primarily consists of alkylphenols, guaiacol, eugenol, hydrocarbons, and other oxygen-containing compounds. Under optimal reaction conditions with Ni/C-H₃[P(Mo₃O₁₀)₄]*13H₂O, the hydrocarbon content surged from 7.5%–95.3%. This significant increase demonstrates the catalyst's robust hydrogenation and deoxygenation capabilities, even for complex bio-oils.

In comparison, Xie et al. reported a 17.9% increase in cycloalkane content in bio-oil using 5% Ni/C at 280 °C, 4 MPa H₂, for 24 h.^[15] and Peng et.al achieved an 83.9% deoxygenation rate for straw bio-oil using Co/NCA_{2.5} at 300 °C, 2 MPa H₂, for 4 h.^[43] Liu et al. increased the hydrocarbon content of bio-oil from 5.74%–39.79% using 2Ru_{2.5}Fe/Al₂O₃ under conditions of 240 °C, 4 h, and 3 MPa H₂.^[44] In comparison, the results obtained in this study surpass those of previous research in terms of effectiveness.

3. Conclusions

In this study, we successfully developed a highly efficient bifunctional catalyst by using green activators to modify peanut shell precursors and preparing biochar with an exceptionally high specific surface area through high-temperature pyrolysis. The unique honeycomb structure of the biochar, characterized by its large surface area and mesopores, facilitated the uniform loading of Ni metal. The incorporation of phosphomolybdic acid provided crucial Brønsted and Lewis acidic sites, significantly enhancing the deoxygenation process. Our experimental results demonstrate that this catalyst achieves highly efficient and selective HDO of guaiacol and other model compounds, with cyclohexane selectivity reaching 97.9% and nearly com-

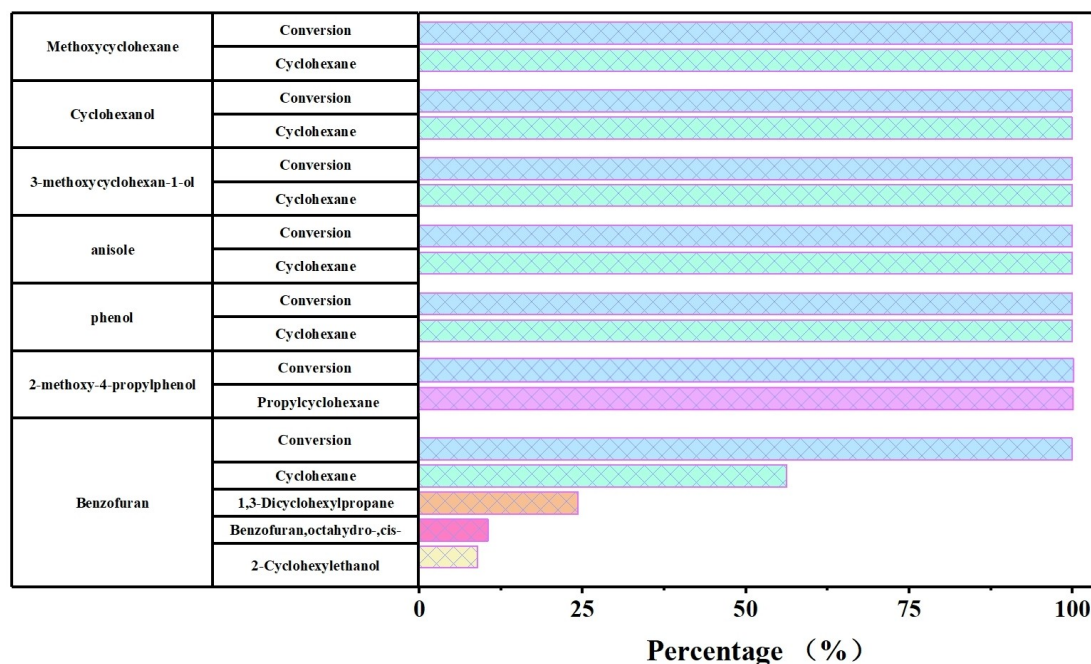


Figure 6. Experimental Results of HDO for Various Model Compounds. (a) Reaction Condition: 50 mg model compounds, 42 mg Ni/C, 20 mg $H_3IP(Mo_2O_{10})_4 \cdot 13H_2O$, 10 mL octane, 240 °C, 1 MPa H_2 , 3 h.

plete hydrocarbon conversion for phenols, ethers, and alcohols. Notably, the bio-oil's hydrocarbon content increased from 7.5% to 95.3%, showcasing the catalyst's superior performance. This indicates a highly effective synergy between the acidic and metal sites within the catalyst, highlighting the importance of the honeycomb-structured biochar in achieving such remarkable HDO efficiency.

Acknowledgements

The authors acknowledge the Young Elite Scientists Sponsorship Program by CAST (2022QNRC001), National Key Technology R&D Program of China (No. 2018YFB1501601), Guangdong Natural Science Foundation (No. 2023 A1515030159) and Open Project of Yunnan Precious Metals Laboratory Co., Ltd (No. YPML-2023050261) for financial supports of this work. NKG expresses gratitude for the startup grant from the Indian Institute of Science (10183) and the financial support provided by the Saroj Poddar Trust through the Saroj Poddar Young Investigator Award.

Conflict of Interests

The authors declare no conflict of interest.

Data Availability Statement

The data that support the findings of this study are available from the corresponding author upon reasonable request.

Keywords: Biochar · Guaiacol · Phenolic compounds · Biomass upgrading · Hydrodeoxygenation · Phosphomolybdic acid

- [1] Y. Wang, A. Akbarzadeh, L. Chong, J. Du, N. Tahir, M.K. Awasthi, *Chemosphere* **2022**, *297*, 134181.
- [2] H. Li, H. Ma, W. Zhao, X. Li, J. Long, *Appl. Energy* **2019**, *253*, 113613.
- [3] S. Chen, Q. Lu, W. Han, P. Yan, H. Wang, W. Zhu, *Fuel* **2021**, *283*, 119333.
- [4] H. Wang, Y. Pu, A. Ragauskas, B. Yang, *Bioresour. Technol.* **2019**, *271*, 449–461.
- [5] S. De, B. Saha, R. Luque, *Bioresour. Technol.* **2015**, *178*, 108–118.
- [6] H. Wang, B. Yang, Q. Zhang, W. Zhu, *Renewable Sustainable Energy Rev.* **2020**, *120*, 109612.
- [7] A. Kumar, A. J. Kumar, T. Bhaskar, *J. Energy Inst.* **2020**, *93*, 235–271.
- [8] X. Diao, N. Ji, X. Li, Y. Rong, Y. Zhao, X. Lu, C. Song, C. Liu, G. Chen, L. Ma, S. Wang, Q. Liu, C. Li, *Appl. Catal. B* **2022**, *305*, 121067.
- [9] T. Yin, Y. Luo, A. S. Chauhan, R. Shu, Z. Tian, C. Wang, Y. Chen, N. K. Gupta, *ChemPhysChem* **2024**, *n/a*, e202400505.
- [10] H. Chen, Y. Chen, J. Liu, B. Hu, Z. Fang, J. Li, Q. Lu, *Ind. Crop. Prod.* **2024**, *214*, 118585.
- [11] Z. Zhang, X. Wang, C. Wang, Z. Yan, G. Zhuang, N. Ma, Q. Li, *Chem. Eng. J.* **2024**, *483*, 149367.
- [12] L. Qu, X. Jiang, Z. Zhang, X. Zhang, G. Song, H. Wang, Y. Yuan, Y. Chang, *Green Chem.: Int. J. Green Chem. Resour.: GC* **2021**, *23*, 9348–9376.
- [13] R. Shu, H. Jiang, L. Xie, X. Liu, T. Yin, Z. Tian, C. Wang, Y. Chen, *Renew. Energy* **2023**, *202*, 1160–1168.
- [14] D. Jiang, M. Lin, Y. Yan, L. Zhan, R. Li, Y. Wu, *Chem. Eng. Sci.* **2024**, *290*, 119779.
- [15] J. Xie, Y. Zhao, Q. Li, L. Qiu, F. Liu, J. Liang, J. Li, J. Cao, *Fuel* **2024**, *371*, 132030.
- [16] Q. Zhang, S. Wang, N. Jiang, B. Jiang, Y. Liu, Y. Chen, F. Li, H. Song, *J. Catal.* **2024**, *432*, 115338.

- [17] S. Dutta, B. Shumeiko, J. Aubrecht, K. Karásková, D. Fridrichová, K. Pacultová, T. Hlinčík, D. Kubička, *J. Catal.* **2024**, *435*, 115553.
- [18] D. Wang, X. Gu, H. Shi, J. Chen, *J. Fuel Chem. Technol.* **2022**, *50*, 1341–1349.
- [19] X. Li, L. Yan, Z. Liu, Y. Liao, L. Ma, *Fuel* **2023**, *338*, 127314.
- [20] A. N. Kay Lup, F. Abnisa, W. M. A. W. Daud, M. K. Aroua, *Chin. J. Chem. Eng.* **2019**, *27*, 349–361.
- [21] C. A. Teles, P. M. de Souza, R. C. Rabelo-Neto, M. B. Griffin, C. Mukar-akate, K. A. Orton, D. E. Resasco, F. B. Noronha, *Appl. Catal., B* **2018**, *238*, 38–50.
- [22] R. Shu, Z. Zhong, H. You, Z. Tian, Y. Chen, L. Ma, *J. Energy Inst.* **2021**, *99*, 1–8.
- [23] G. Novodárszki, F. Lónyí, B. Csík, M. R. Mihályi, R. Barthos, J. Valyon, A. Vikár, D. Deka, Z. Pászti, Y. Shi, H. E. Solt, *Appl. Catal., A* **2024**, *680*, 119757.
- [24] Q. Zhang, S. Wang, N. Jiang, B. Jiang, Y. Liu, Y. Chen, F. Li, H. Song, *J. Catal.* **2024**, *432*, 115338.
- [25] L. Znak, J. Zieliński, *Appl. Catal. A* **2008**, *334*, 268–276.
- [26] X. Chen, Q. Zhang, S. Li, H. Wang, X. Zhang, L. Chen, L. Ma, J. Liu, *Fuel Process. Technol.* **2024**, *258*, 108095.
- [27] S. Dutta, B. Shumeiko, J. Aubrecht, K. Karásková, D. Fridrichová, K. Pacultová, T. Hlinčík, D. Kubička, *J. Catal.* **2024**, *435*, 115553.
- [28] W. O. Makinde, M. A. Hassan, Y. Pan, G. Guan, N. López-Salas, A. S. G. Khalil, *J. Alloy. Compd.* **2024**, *991*, 174452.
- [29] V. P. Mahajan, Y. A. Kolekar, B. M. Bhanage, *Mol. Catal.* **2024**, *561*, 114167.
- [30] P. Yan, X. Tian, E. M. Kennedy, M. Stockenhuber, *Catal. Sci. Technol.* **2022**, *12*, 2184–2196.
- [31] F. Yang, D. Liu, Y. Zhao, H. Wang, J. Han, Q. Ge, X. Zhu, *ACS Catal.* **2018**, *8*, 1672–1682.
- [32] S. Lv, X. Liu, X. Shen, *Surf. Sci.* **2022**, *718*, 122015.
- [33] Z. Jia, N. Ji, X. Diao, X. Li, Y. Zhao, X. Lu, Q. Liu, C. Liu, G. Chen, L. Ma, S. Wang, C. Song, C. Li, *ACS Catal.* **2022**, *12*, 1338–1356.
- [34] Y. Zhang, T. Liu, H. Jia, Q. Xia, X. Hong, G. Liu, *Catal. Sci. Technol.* **2022**, *12*, 3343–3426.
- [35] R. Huang, J. Jiang, J. Liang, S. Wang, Y. Chen, X. Zeng, K. Wang, *Green Energy Environ.* **2024**.
- [36] C. Wen, S. Li, P. Zhang, M. Lu, J. Zhu, M. Li, C. Song, *Biomass Bioenerg.* **2024**, *187*, 107289.
- [37] Y. Khani, A. Kumar, B. Sung Kang, C. Hyun Ko, M. Ali Khan, B. Jeon, Y. Park, *Chem. Eng. J. (Lausanne, Switzerland)* **1996**, *490*(2024), 151637.
- [38] H. Zhang, T. Yang, Y. Tong, B. Li, J. Wang, R. Li, *Fuel* **2024**, *368*, 131620.
- [39] X. Chen, B. Luo, J. Wang, J. Liu, C. Wang, Z. Tian, R. Shu, Y. Chen, *J. Energy Inst.* **2024**, *114*, 101584.
- [40] Z. Xiang, W. Wang, F. Zhou, H. Zhang, Y. Wang, W. Zhu, H. Wang, *Fuel Process. Technol.* **2024**, *256*, 108073.
- [41] J. Xu, P. Zhu, I. H. El Azab, B. Bin Xu, Z. Guo, A. Y. Elnaggar, G. A. M. Mersal, X. Liu, Y. Zhi, Z. Lin, H. Algadi, S. Shan, *Chin. J. Chem. Eng.* **2022**, *49*, 187–197.
- [42] S. Pérez, A. Moreno, Z. Du, D. López, *Fuel Process. Technol.* **2022**, *236*, 107416.
- [43] Q. Peng, X. Jiang, G. Cao, T. Xie, Z. Jin, L. Xie, F. Gan, S. Ma, M. Peng, *Bioresour. Technol.* **2024**, *406*, 131059.
- [44] T. Liu, Z. Tian, W. Zhang, B. Luo, L. Lei, C. Wang, J. Liu, R. Shu, Y. Chen, *Fuel* **2023**, *339*, 126916.

Manuscript received: August 14, 2024

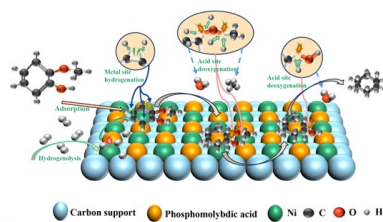
Revised manuscript received: September 26, 2024

Accepted manuscript online: October 9, 2024

Version of record online: ■■, ■■

RESEARCH ARTICLE

A bifunctional catalyst comprising Ni nanoparticles and phosphomolybdic acid supported on three-dimensional honeycomb biochar is developed for hydrodeoxygenation of guaiacol. The catalyst exhibits high activity, achieving 100% guaiacol conversion and 97.9% cyclohexane selectivity. The porous biochar structure ensures uniform Ni dispersion, while phosphomolybdic acid acts as a homogeneous catalyst, enhancing the overall catalytic efficiency by facilitating a heterogeneous-homogeneous catalytic reaction.



T. Yin, Y. Luo, R. R. Nayak, R. Shu*, Z. Tian, C. Wang, Y. Chen, N. K. Gupta*

1 – 9

Highly Efficient and Selective Hydrodeoxygenation of Guaiacol Using Ni-Supported Honeycomb-Structured Biochar and Phosphomolybdic Acid

